Vibration Characteristics of Rotor System with Loose Disc Caused by the Insufficient Interference Force

Zhi-Nong Li (lizhinong@tsinghua.org.cn)
Key Laboratory of Nondestructive Testing, Ministry of Education, Nanchang Hangkong University, China
Fang Qiao
Nanchang Hangkong University
Wen Xiu Lu
Tsinghua University
Jie Liu
Nanchang Hangkong University
Dong Wang
Shanghai Jiao Tong University
Fu Lei Chu
Tsinghua University

Original Article

Keywords: rotor system with loose disc, rotor dynamics, nonlinear dynamic characteristic, nonlinear vibration, insufficient interference force, fault diagnosis

Posted Date: June 4th, 2020

DOI: https://doi.org/10.21203/rs.3.rs-31916/v1

Title page

Vibration Characteristics of Rotor System with Loose Disc Caused by the Insufficient Interference Force

Zhi-Nong Li, born in 1966, is currently a professor at *Key Laboratory of Nondestructive Testing*, *Ministry of Education, Nanchang Hangkong University, China.* He received his PhD degree from *Zhejiang University, China,* in 2003. His research interests include intelligent detection and signal processing, mechanical vibration and control.
E-mail: lizhinong@tsinghua.org.cn

Fang Qiao, born in 1995, is currently a graduate student at *Nanchang Hangkong University, China.*
E-mail: 1654511145@qq.com

Wen-Xiu Lu, born in 1974 , is currently an associate professor at *Tsinghua university, China*. He received his PhD degree from *Tsinghua University, China,* in 2002.
E-mail:luwenxiu@tsinghua.edu.cn

Jie liu,born in1991, is a graduate student at *Nanchang Hangkong University,* China,in 2018.
E-mail:846664936@qq.com

Dong Wang, born in 1984, is currently an associate professor at *State Key Laboratory of Mechanical Systems and Vibration, Shanghai Jiaotong University, China.* He received his PhD degree from *City University of Hong Kong, China,* in 2015.
E-mail: dongwang4-c@sjtu.edu.cn

Fu-Lei Chu, born in 1959, is a professor at *Tsinghua University, China.* He received his PhD degree from *Southampton university, England,* in 1993.
E-mail: chufulei@cueb.edu.cn

Corresponding author：Zhi-Nong Li　E-mail：lizhinong@tsinghua.org.cn

Vibration Characteristics of Rotor System with Loose Disc Caused by the Insufficient Interference Force

Zhinong LI [1], Fang QIAO [1], Wenxiu LU [2], Jie LIU [1], Dong WANG [3], Fulei CHU[2]

1. Key Laboratory of Nondestructive Testing, Ministry of Education, Nanchang Hangkong University, Nanchang 330063, China;
2. Department of Mechanical Engineering, Tsinghua University, Beijing 100084, China;
3. The State Key Laboratory of Mechanical Systems and Vibration, Shanghai Jiaotong University, Shanghai, 200240, China

Corresponding author: Zhinong LI, Email: lizhinong@tsinghua.org.cn

Abstract: The loose of mechanical parts is one of the common failures in rotating machinery. The current researches of loose fault mainly focus on non-rotating components. However, the loose of disc, which is the main work part in the rotor system, is less paid attention, and the mechanism and dynamics characteristics of the loose fault are also almost ignored. In this paper, a dynamic contact model of the rotor system with loose disc is established considering the microscopic surface topography. Through the numerical simulation, the vibration characteristics of the disc-shaft rotor system are analyzed and discussed. The simulation results are further verified by experiments. The results show that the rotation state of the disc is affected by the rotation speed of the shaft, contact stiffness, a gap between the disc and shaft, damping of the disc, and the rotational damping. When the speed difference between the disc and shaft is zero or large, the collision frequency is mainly composed of one frequency component. When the rotational speed of the disc approaches the shaft, the beating vibration phenomenon of the disc occurs in the horizontal direction. As the decreases of relative speed between the disc and shaft, the disc trajectory changes from ‘circular’ to ‘double ring’ and then ‘circular’. The research results on nonlinear dynamics characteristics of the loose disc has important theoretical value and practical application value, and makes up for its shortcomings in the rotor system with loose disc.

Keywords: Rotor system with loose disc; Rotor dynamics; Nonlinear dynamic characteristic; Nonlinear vibration; Insufficient interference force; Fault diagnosis

1. Introduction

Loose fault of mechanical parts, which is one of the common failures in the rotor system,

interferes with the normal operation of the rotor system, resulting in the decreasing of mechanical power and even machine malfunction. In general, mechanical looseness includes pedestal looseness, loose base and so on. For a double-disc single-span rotor system with pedestal looseness fault, Ma et al [1] analyzed the influence of the stiffness of bolt without looseness, looseness gap, and rotational speed on the dynamic characteristics of the system using three dimensional spectrums and shaft center trajectory. Sun et al [2] established a finite element model that can characterize complex structures and validated the model by comparing critical speed and mode shape. In Ref. [3], a rotor model with nonlinear oil film force was established and solved by the numerical method of Runge-Kutta to obtain frequency characteristics of the rotor system. In Ref. [4], a model of the rotor system with looseness and rub-impact faults was established. Based on the nonlinear finite element method and the contact theory, the dynamics characteristics of the system were studied by considering the effects of the looseness stiffness and the clearance between rotor and stator. Based on nonlinearity measure, Mian et al [5] proposed a method to evaluate the pedestal looseness of bearing-rotor system under constant rotational speed, where piecewise-linear stiffness, damping force, and nonlinear elastic force were considered.

The existing research on non-rotating components mainly focus on the coupling failure and vibration characteristics [6-11]. However, there are few studies on rotating parts. At present, Behzad [12-13] made a preliminary exploration on the rotor system with loose disc. In that work, the model of the looseness of disc-shaft with large clearance was established based on the premise that the rotating speed of the disc is assumed to be constant, the disc and the shaft is always in contact state. The model ignored the collision and friction between the disc and rotating shaft and assumed that the disc and the rotating shaft run at the same speed. So, this assumption is unrealistic. These conditions are also inconsistent with the actual conditions. In actual case, the phenomenon of the rotor system with loose disc generally only occurs when the clearance is small or there is no gap. When the interference between the disc and shaft is insufficient or the deflection of the high-speed rotor increases due to mass imbalance or bending, a relative sliding between the disc and shaft occur. The sliding affects the dynamic characteristics of the whole rotor system.

Therefore, based on the contact model of disc-shaft considering the microscopic surface morphology, the motion differential equations of the rotor system with loose disc caused by the

insufficient interference force [14] is established and is simulated by numerical method. The rotation state of the disc is affected by the rotation speed of the shaft, contact stiffness, gap, damping of the disc, and the rotational damping. The motion characteristics of the disc are determined through analyzing the changes of the waveform diagrams in the horizontal direction, the spectrograms, and the difference between the disc and shaft in vibration displacement. The influence of the rotation speed on the disc trajectory is discussed [15-17]. Finally, the simulation results are verified by experiments.

2. Mathematical Model

2.1 the contact model of disc-shaft

Figure 1 is a schematic diagram of disc-shaft contact [18]. In Figure 1, the outer circle represents the disc and the inner circle represents the rotating shaft. It is assumed that the height of the micro-protrusion between the inner circle and outer circle is negligible. o_1 and r_1 are the centroid and radius of the shaft, and o_2 and r_2 are the centroid and radius of the disc, respectively. The extension line of o_1o_2 intersects the shaft and disc at point P and point Q, respectively. After φ rotation of the extension line, the intersection with the rotation shaft and the disc are point B and point C, respectively.

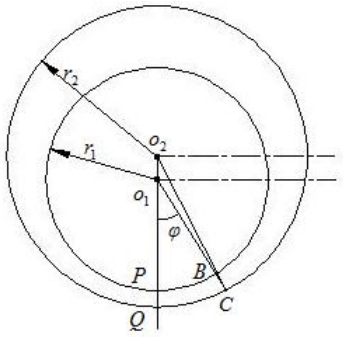

Figure 1 The schematic diagram of disc -shaft contact

In the triangle Δo_1o_2C, the straight line $\overline{o_1o_2}$ is the relative distance (r) between the disc and shaft, and $\overline{o_2C} = r_2$. Then, according to cosine theorem, o2C can be written as

$$\overline{o_2C}^2 = \overline{o_1o_2}^2 + \overline{o_1C}^2 - 2\overline{o_1o_2}\,\overline{o_1C}\cos\angle o_1o_2C \tag{1}$$

The formula (1) can be simplified as

$$r_2^2 = r^2 + \overline{o_1C}^2 + 2r\overline{o_1C}\cos\varphi \tag{2}$$

Then, at any angle φ, the gap between the disc and shaft is

$$\Delta d(\varphi) = \overline{o_1 C} - r_1 = \sqrt{r_2^2 - r^2 \sin^2 \varphi} - r\cos\varphi - r_1 \tag{3}$$

The contact normal force is generated only when the height of micro-protrusion z is higher than $\Delta d(\varphi)$. The normal force generated by the micro-protrusion is written

$$\Delta F = 4E'\gamma^{1/2}\left(z - \Delta d(\varphi)\right)^{3/2} / 3 \tag{4}$$

$$1/\gamma = 1/\gamma_1 + 1/\gamma_2 \tag{5}$$

$$1/E' = 1/E_1 + 1/E_2 \tag{6}$$

where γ_1 is the radius of the disc, γ_2 is the radius of the shaft, γ is the radius of the micro-protrusion, E_1 is the elastic modulus of the disc, E_2 is the elastic modulus of the shaft, and E is the elastic modulus of the micro-protrusion. It is assumed that the normal distribution function of z on the contact surface is $\Phi(z)$, the mean of normal force at any angle φ is expressed

$$\overline{\Delta F}(\varphi) = \int_{\Delta d(\varphi)}^{\infty} \Delta F \Phi(z) dz \tag{7}$$

The micro-protrusion has the density of η and the length of $r_1 d(\varphi)$. So, on the micro-area segment with a width of l, the number of micro-protrusions is $\eta l r_1 d\varphi$. According to the principle of calculus, the total force on the entire contact surface is

$$F = \int_0^{2\pi} \overline{\Delta F} d\varphi = 4/3 l\eta r_1 E'\gamma^{1/2} \int_0^{2\pi}\int_{\Delta d(\varphi)}^{\infty} [z - \Delta d(\varphi)]\Phi(z) dz d\varphi \tag{8}$$

Since the contact force is symmetric with respect to $o_1 o_2$, the formula (8) can be simplified as

$$F = \frac{8}{3} l\eta r_1 E'\gamma^{1/2} \int_0^{\pi}\int_{\Delta d(\varphi)}^{\infty} [z - \Delta d(\varphi)]\Phi(z) dz d\varphi \tag{9}$$

The radial force generated by a single micro-protrusion at any angle φ is $\Delta F_r = \Delta F \cos\varphi$. So, the mean is $\overline{\Delta F_r}(\varphi) = \overline{\Delta F(\varphi)}\cos\varphi$. Therefore, the total radial force generated over the entire circumference is

$$F_r = \frac{8}{3} l\eta r_1 E'\gamma^{1/2} \int_0^{\pi}\int_{\Delta d(\varphi)}^{\infty} [z - d(\varphi)]\Phi(z)\cos\varphi dz d\varphi \tag{10}$$

During the contact between the disc and shaft, it is assumed that the contact of each micro-protrusion meets the Coulomb law of friction. Let μ is the friction coefficient at the

contact point, and $\Delta\omega = \omega_1 - \omega_2$ (ω_1 is the rotation speed of the disc, ω_2 is the rotation speed of the shaft). So, the tangential force generated by a single micro-protrusion at any angle φ is $\Delta F_t = \mathrm{sgn}(\Delta\omega)\Delta F\cos\varphi$. Then, the mean of the tangential force is $\Delta\overline{F_t}(\varphi) = \mathrm{sgn}(\Delta\omega)\Delta\overline{F}(\varphi)\cos\varphi$. So, the total tangential force generated over the entire circumference is

$$F_t = \mathrm{sgn}(\Delta\omega)\frac{8}{3}\mu l\eta r_1 E'\gamma^{1/2}\int_0^{\pi}\int_{\Delta d(\varphi)}^{\infty}[z-\Delta d(\varphi)]\Phi(z)\cos\varphi dz d\varphi \tag{11}$$

where $\mathrm{sgn}(\Delta\omega)$ is the step function, which is

$$\mathrm{sgn}(\Delta\omega) = \begin{cases} 1, \Delta\omega > 0 \\ 0, \Delta\omega = 0 \\ -1, \Delta\omega < 0 \end{cases} \tag{12}$$

The frictional force F_f generated by the entire contact surface of disc-shaft be expressed as follows.

$$F_f = \mathrm{sgn}(\Delta\omega)\mu F \tag{13}$$

The force components of the disc on the shaft in two coordinate axes are

$$\begin{Bmatrix} F_x \\ F_y \end{Bmatrix} = -\frac{1}{r}\begin{bmatrix} F_r & -F_t \\ -F_t & F_r \end{bmatrix}\begin{Bmatrix} x_1 - x_2 \\ y_1 - y_2 \end{Bmatrix} \tag{14}$$

2.2 The motion equations of the rotor system with loose disc

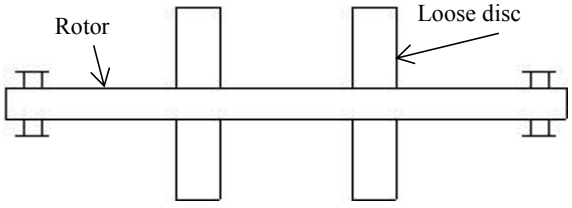

Figure 2 The model of the rotor system with loose disc

Figure 2 shows the rotor system with concentrated mass [19]. In the case of ignoring the gyroscopic effect, the contact model of disc-shaft considering the topography of microscopic surface is more advantageous for analysis. The disc slides relative to the shaft due to the external load produced by the insufficient interference force between the disc and shaft. The external load generally has great influence on the disc-shaft system. Therefore, this paper uses the model of disc with nonlinear rotational damping.

The vibration equations of the shaft are

$$\begin{cases} m_1\ddot{x}_1 + c_1\dot{x}_1 + kx_1 = m_1e_1\omega^2\cos(\omega t) + f_x \\ m_1\ddot{y}_1 + c_1\dot{y}_1 + ky_1 = m_1e_1\omega^2\sin(\omega t) - m_1g + f_y \end{cases} \tag{15}$$

Where m_1, c_1 and k are the mass, damping coefficient and stiffness coefficient of the shaft, e_1 and ω are the eccentric distance and the rotation speed of the shaft, respectively. f_x and f_y are the components of the force acting on the rotating shaft by the disc in the x and y directions, respectively.

The vibration equations of the disc are

$$\begin{cases} m_2\ddot{x}_2 + c_2\dot{x}_2 = m_2e_2\dot{\theta}^2\cos\theta + m_2e_2\ddot{\theta}\sin\theta - f_x \\ m_2\ddot{y}_2 + c_2\dot{y}_2 = m_2e_2\dot{\theta}^2\sin\theta - m_2e_2\ddot{\theta}\cos\theta - m_2g - f_y \end{cases} \tag{16}$$

where m_2, c_2 and e_2 are the mass, the vibration damping coefficient, and the eccentric distance of the disc, respectively [20-21].

The rotational vibration equation of the disc is

$$j\ddot{\theta} + c_3\dot{\theta}^2 = f_t r_2 - m_2 g e_2\cos\theta \tag{17}$$

where j, and c_3 are the moment of inertia and the rotational damping coefficient of the disc, respectively.

For the sake of convenience, the above-mentioned model is pertinently dimensioned. The equations of motion after dimensionless are

$$\begin{cases} \ddot{X}_1 = E_1\cos\tau + \dfrac{F_x}{\Omega^2} - \dfrac{\xi_1}{\Omega}\dot{X}1 - \dfrac{K}{\Omega^2}X_1 \\ \ddot{Y}_1 = E_1\sin\tau - \dfrac{G}{\Omega^2} + \dfrac{F_y}{\Omega^2} - \dfrac{\xi_1}{\Omega}\dot{Y}_1 - \dfrac{k}{\Omega^2}Y_1 \\ \ddot{X}2 = E_2\dot{\theta}^2\cos\theta + E_2\ddot{\theta}\sin\theta - \dfrac{F_x}{s\Omega^2} - \dfrac{\xi_2}{S\Omega}\dot{X}_2 \\ \ddot{Y}_2 = E_2\dot{\theta}^2\sin\theta - E_2\ddot{\theta}\cos\theta - \dfrac{F_y}{s\Omega^2} - \dfrac{\xi_2}{S\Omega}\dot{Y}_2 - \dfrac{G}{\Omega^2} \\ \ddot{\theta} = F_tR^2\dfrac{1}{j\Omega^2} - SG\dfrac{1}{j\Omega^2}E_2\cos\theta - \dfrac{\xi_3}{j}\dot{\theta}^2 \end{cases} \tag{18}$$

where $\tau=\omega t$, $X_i=x_i/\sigma$, $Y_i=y_i/\sigma$, $\dot{X}_i=dx_i/d\tau$, $\dot{Y}_i=dy_i/d\tau$, $\ddot{X}_i=d\dot{X}_i/d\tau$, $\ddot{Y}_i=d\dot{Y}_i/d\tau$, $\omega_0=\sqrt{k/(m_1+m_2)}$, $\Omega=\omega/\omega_0$, $E_1=e_1/\sigma$, $E_2=e_2/\sigma$, $\xi_1=c_1/m_1\omega_0$, $\xi_2=c_2/m_2\omega_0$, $\xi_3=c_3/m_3\sigma_2$, $K=k/m_1\omega_0^2$, $G=g/\omega_0^2\sigma$, $F_x=f_x/m_1\omega_0^2\sigma$, $F_y=f_y/m_1\omega_0^2\sigma$, $J=j/m_1\sigma_2$, $S=m_2/m_1$, $C=4/3l\eta r_1E'\sigma\sqrt{2\sigma\gamma/\pi}$. σ is the root mean square of the micro-protrusion distribution on the disc-shaft contact surface.

In Figure 2, the model is composed of a simple rotor and a loose disc, while the rotor with concentrated mass is rigidly supported. According to the research results of Behzad, the gyroscopic effect is ignored in the analysis because it has little influence on the system results.

At the same time, the fourth-order Runge-Kutta [22-23] method is used to solve the equations (18). In order to ensure the convergence of the solution and reduce the calculation error, the time step of the solution is set to $\pi/640$.

3 Numerical analysis

3.1 Analysis of motion state of the disc

When the loose failure occurs, the rotation speed of the disc is no same as the shaft, and the motion state of the disc inevitably change. Therefore, studying the motion state of the disc is the key to studying the rotor system with loose disc. It be known from equations (10), (11), (13) and (18) that the motion characteristics of the system are affected by the rotation speed of shaft (Ω), the contact stiffness (C), gap (H), the damping of disc (ξ_2), and the rotational damping (ξ_3) , E_1 and E_2 , the rotation speed of disc $\theta_1^{'}$ and so on. Therefore, the motion state of the disc is discussed by the above several factors.

(1) Influence of shaft speed

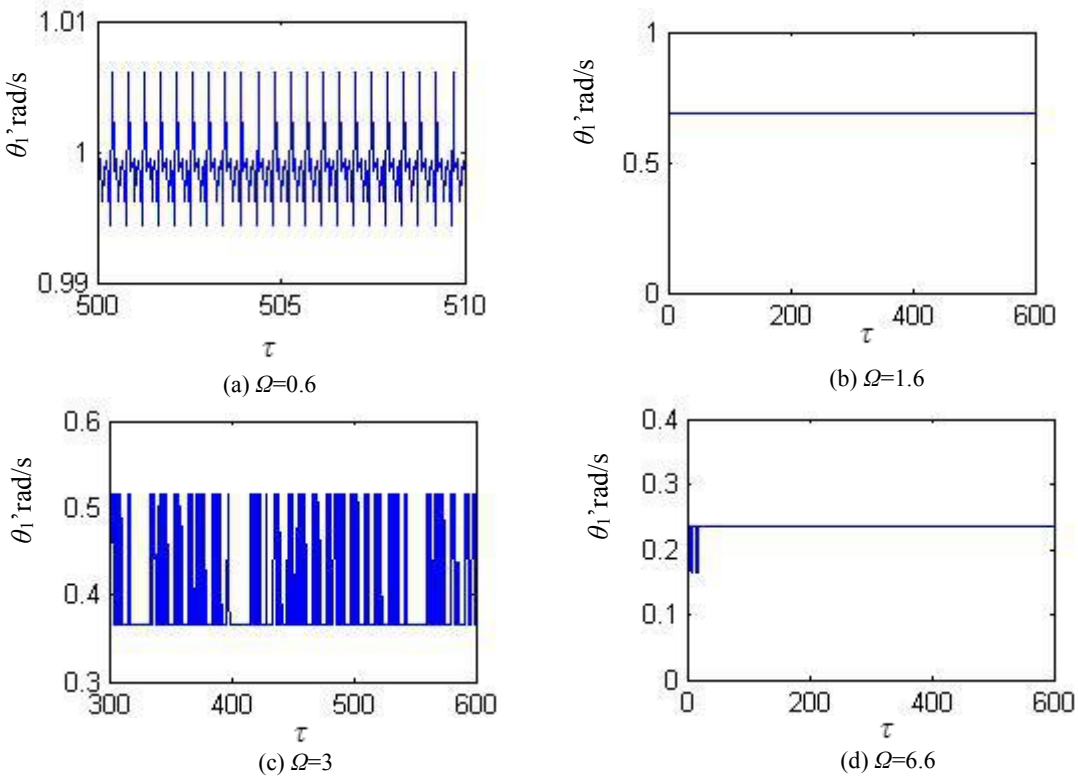

Figure 3 The changing diagram of θ_1' at different Ω

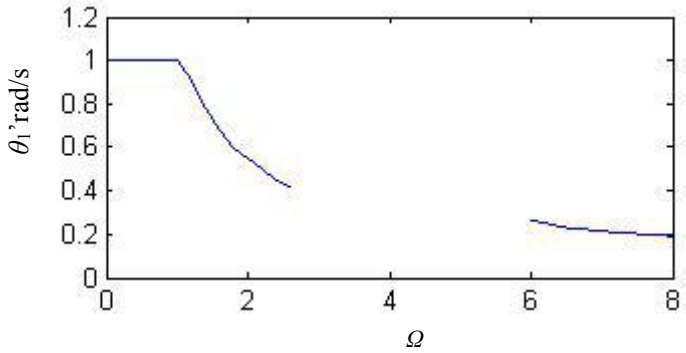

Figure 4 The changing diagram of θ_1' with Ω
(The unmarked part indicates that θ_1' is in a surge state)

The change of θ_1' at different Ω is shown in Figure 3. Through analysis, it is found that when $\Omega \leq 1$, the shaft speed is basically the same as the speed of the disc. When $1 < \Omega \leq 2.6$, θ_1' decreases with the increase of Ω. When $2.6 < \Omega \leq 5.8$, the rotation speed of the disc is no longer stable and in a state of surge, θ_1' decreases with the increase of Ω. When $5.8 < \Omega$, the rotation speed of the disc returns to a steady state, and the θ_1' continues to decrease with the increase of Ω. Figure 4 is the changing diagram of θ_1' with Ω. As shown in Figure 4, when Ω is low, the disc and the shaft basically run at the same speed. With the increasing of Ω, θ_1' decreases

gradually.

(2) Influence of the contact stiffness (C value) of disc-shaft

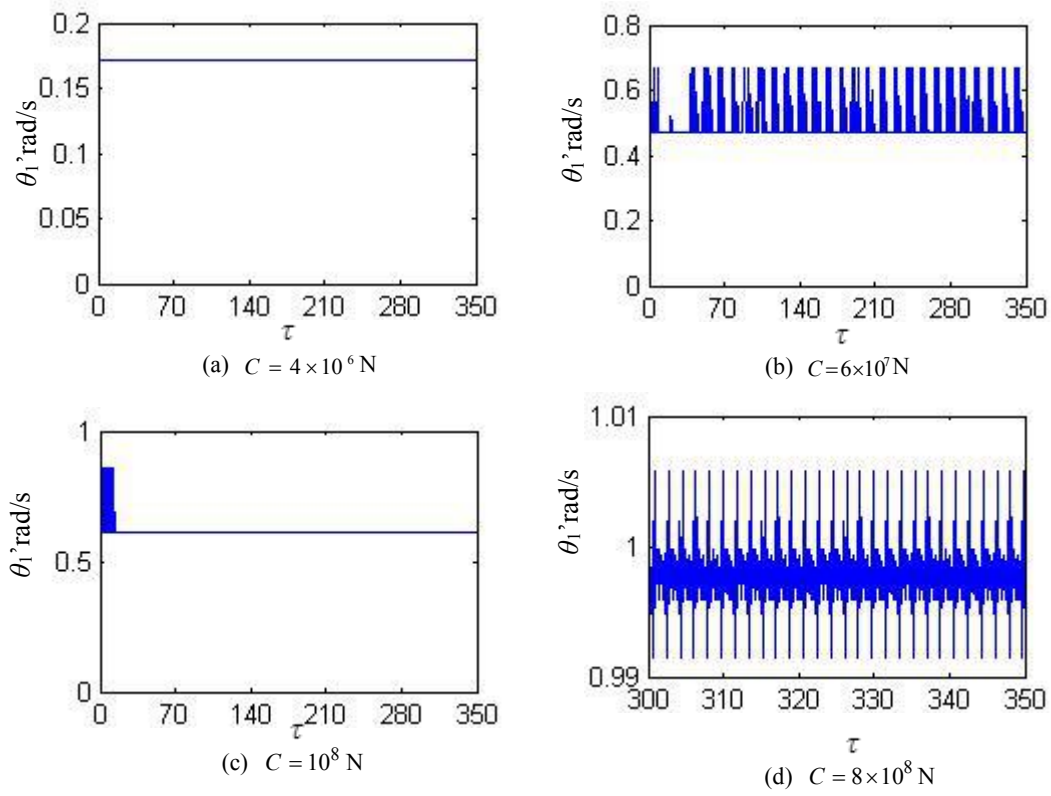

(a) $C = 4\times10^6$ N (b) $C=6\times10^7$ N

(c) $C = 10^8$ N (d) $C = 8\times10^8$ N

Figure 5 The changing diagram of θ_1' at different C

Let $C = 4/3l\eta r_1 E^{'}\sigma\sqrt{2\sigma\gamma/\pi}$, C has the linear relationship with the contact stiffness of disc-shaft. Therefore, the influence of the elastic modulus on the motion state of the disc is known by discussed the influence of C on the motion state of the disc.

It can be known from the analysis, when $C \le 4\times10^6 N$, with the increase of C, θ_1' gradually increased. When $4\times10^6 < C \le 6\times10^7 N$, the rotational speed of the disc is in the state of surge, and with the increases of C, θ_1' gradually increases. When $6\times10^7 < C \le 3\times10^8 N$, the rotation speed of the disc has returned to stability, and with the increases of C, θ_1' continues to increase. When $C > 3\times10^8 N$, the rotation speed of the disc is the same as the rotation speed of the shaft. With the increase of C, the rotation state of the disc is more stable. The process of increasing C is the process of increasing the contact stiffness, increasing the interference force and lightening the loose fault of the disc-shaft, so that the rotation speed of the disc is getting more stable.

(3) Influence of the disc-shaft clearance H

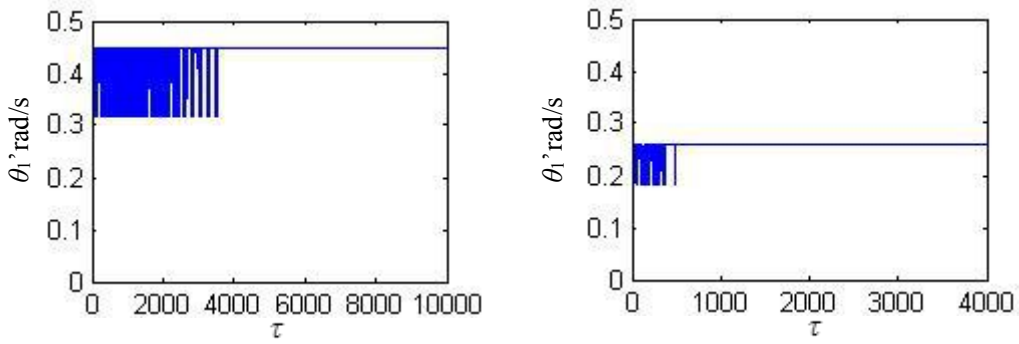

(a) H=1μm (b) H=1.5μm

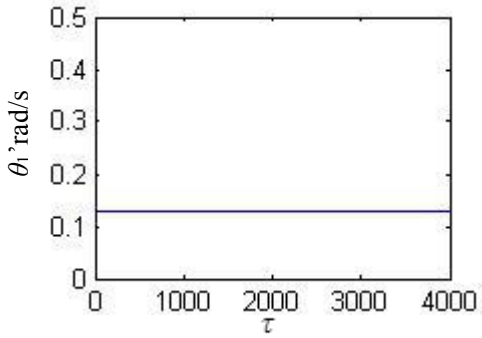

(c) H=2μm

Figure 6 The changing diagram of θ_1' at different H

It can be known from Figure 6 that with the increases of H, θ_1' gradually decreases. The reason for this phenomenon is that the interference force of disc-shaft system gradually decreases with the increases of H. The influence effect of the interference force is consistent with the rotation speed of the shaft and the contact stiffness of disc-shaft.

(4) Influence of damping

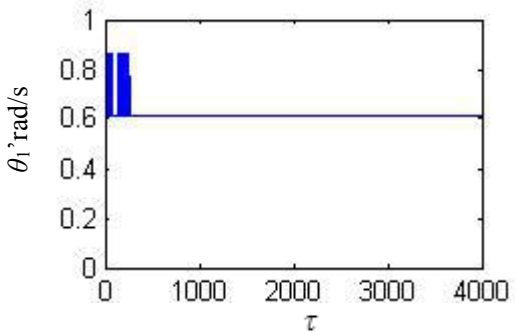

Figure 7 The changing diagram of θ_1' when $\xi_1 = 1/3$

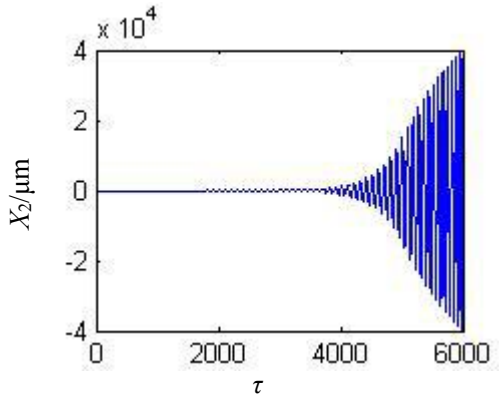

(a) The Waveform of X_2

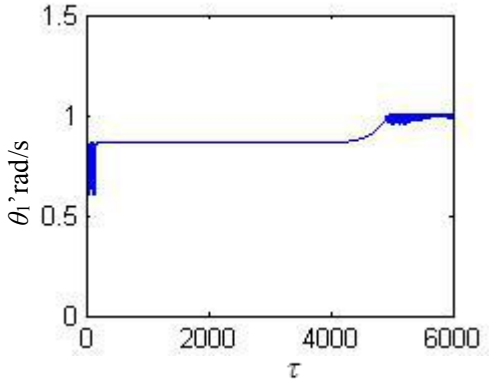

(b) The changing diagram of θ_1'

Figure 8 The changing diagram of motion state of disc when $\xi_2 = 0.1$

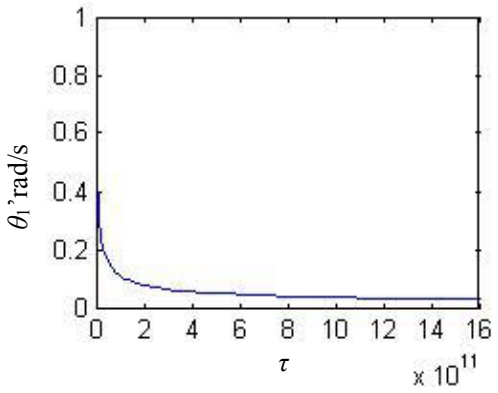

Figure 9 The changing diagram of θ_1' with ξ_3

Firstly, the influence of ξ_1 is analyzed, under $\xi_2 = 2$ and $\xi_3 = 1/3 \times 10^9$. With the change of ξ_1, the simulation result demonstrates that the rotation state of the disc is almost constant, that is, the motion state of the disc is not sensitive to the change of ξ_1. Then, the influence of ξ_2 is analyzed under $\xi_1 = 1/3$ and $\xi_3 = 1/3 \times 10^9$. With the change of ξ_2, the simulation result found that when $\xi_2 \geq 12$, θ_1' is always stable at 0.61. However, when $\xi_2 \leq 12$, the vibration amplitude of the disc gets larger, the rub-impact of the disc-shaft gets more intense, the rotation speed of the disc is sharply increased from a certain value lower than the rotational speed of the shaft to the vicinity at the rotational speed of the shaft, and the increase sharply in the disc speed is simultaneous with the vigorous vibration of the disc. The vigorous change of the disc-shaft rubbing causes the frictional force to change drastically, and thereby causes θ_1' to fluctuate at one point. Figure 8 is the change diagram of motion state of disc when $\xi_2 = 0.1$. It can be seen that

the amplitude of the disc is particularly large at this time, and still in increasing state, which is obviously in an abnormal state.

Finally, the influence ξ_3 is analyzed under the conditions of $\xi_1 = 1/3$ and $\xi_2 = 2$. The simulation result shows that with the increase of ξ_3, θ_1' gradually decreases. When ξ_3 is small, θ_1' decreased rapidly, and when ξ_3 is larger, θ_1' decreased slowly. The greater the rotational damping, the lower the rotational speed of the disc.

In summary, the motion state of the disc is affected by Ω, the contact stiffness, H, ξ_2, and ξ_3. The system changes less and are more stable than the disc-shaft system with large looseness.

3.2 Analysis of time-frequency characteristics

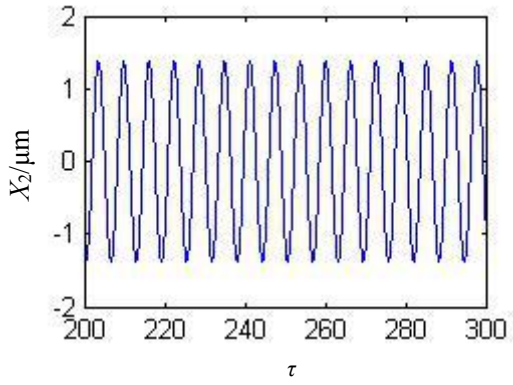

(a) The waveform of X_2

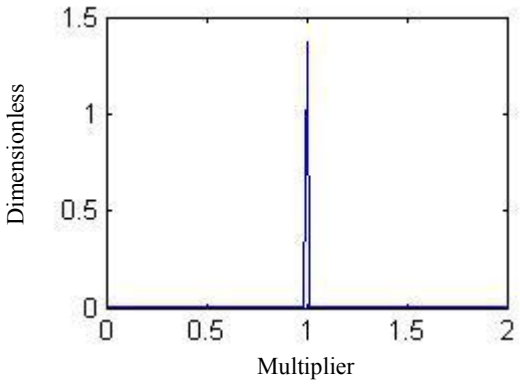

(b) The spectrogram of X_2

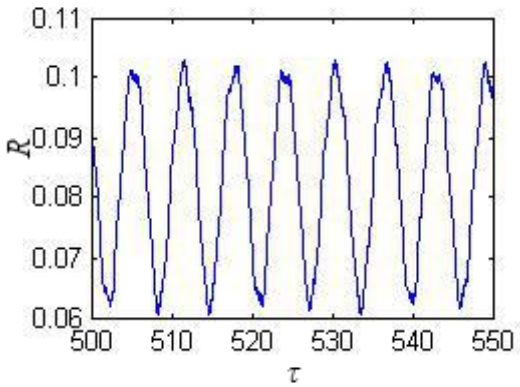

(c) The waveform of R

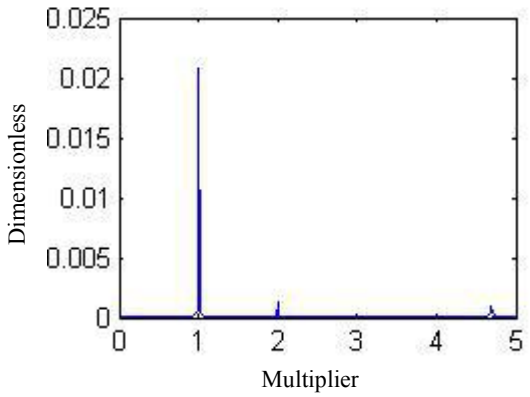

(d) The spectrogram of R

Figure 10 Time-frequency diagram of the disc-shaft at the same speed

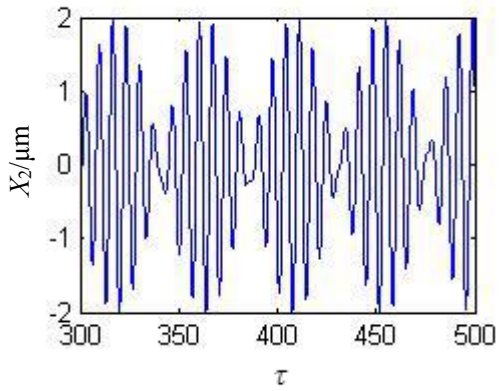

(a) The waveform of X_2

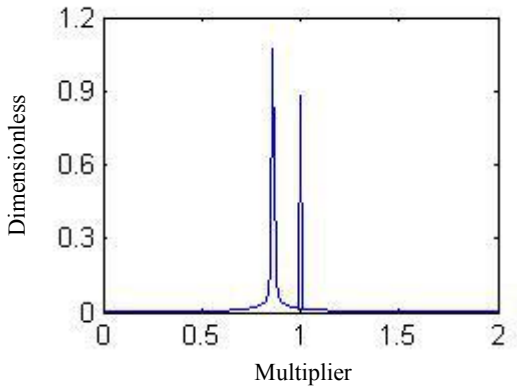

(b) The spectrogram of X_2

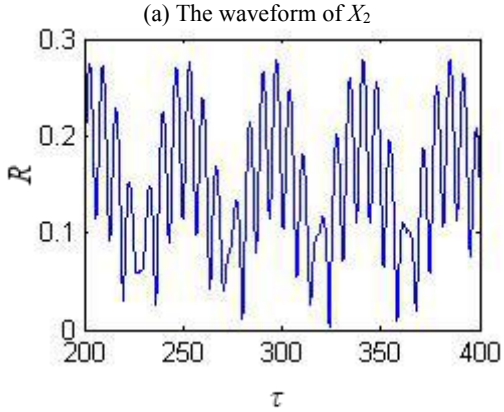

(c) The waveform of R

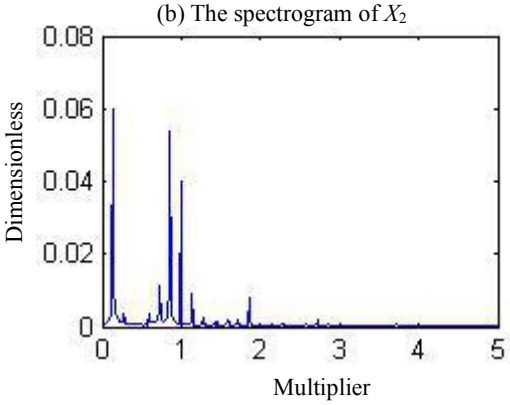

(d) The spectrogram of R

Figure 11 Time-frequency diagram when $\theta_1' = 0.86$

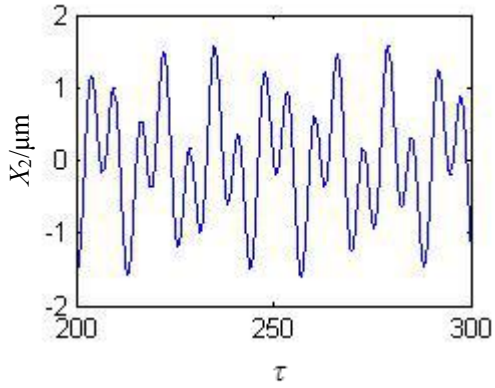

(a) The waveform of X_2

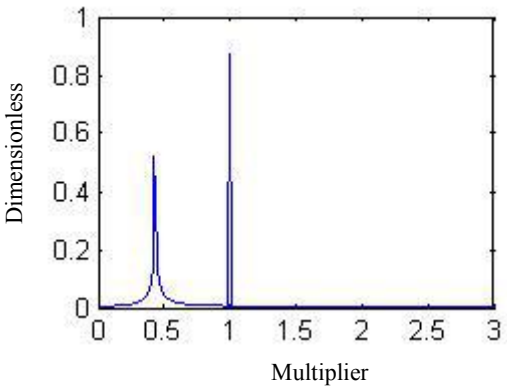

(b) The spectrogram of X_2

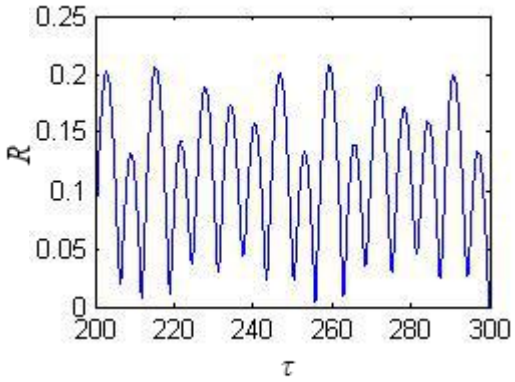

(c) The Waveform of R

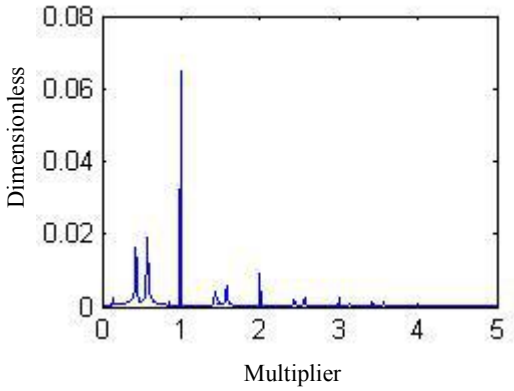

(d) The spectrogram of R

Figure 12 Time-frequency diagram when $\theta_1' = 0.42$

Figure. 10 is the time-frequency diagrams of the disc-shaft at the same speed. It can be seen from the spectrogram of X_2 that only one frequency component is included. Figure. 11 is the time-frequency diagrams when $\theta_1' = 0.86$. It can be seen from the spectrogram of X_2 that it contains the rotating frequency of the disc and the shaft. Since the rotating frequency of the disc and the shaft are close, the beating vibration phenomenon in the X_2 waveform diagram appears. The spectrogram of R is mainly composed of a low frequency and a small high frequency component. Figure. 12 is the time-frequency diagram when $\theta_1' = 0.42$. It can be seen from the spectrogram of X_2 that it contains the rotating frequency of the disc and the shaft. The spectrogram of R is mainly composed of one frequency, small high frequency and low frequency components.

3.3 Motion trajectory

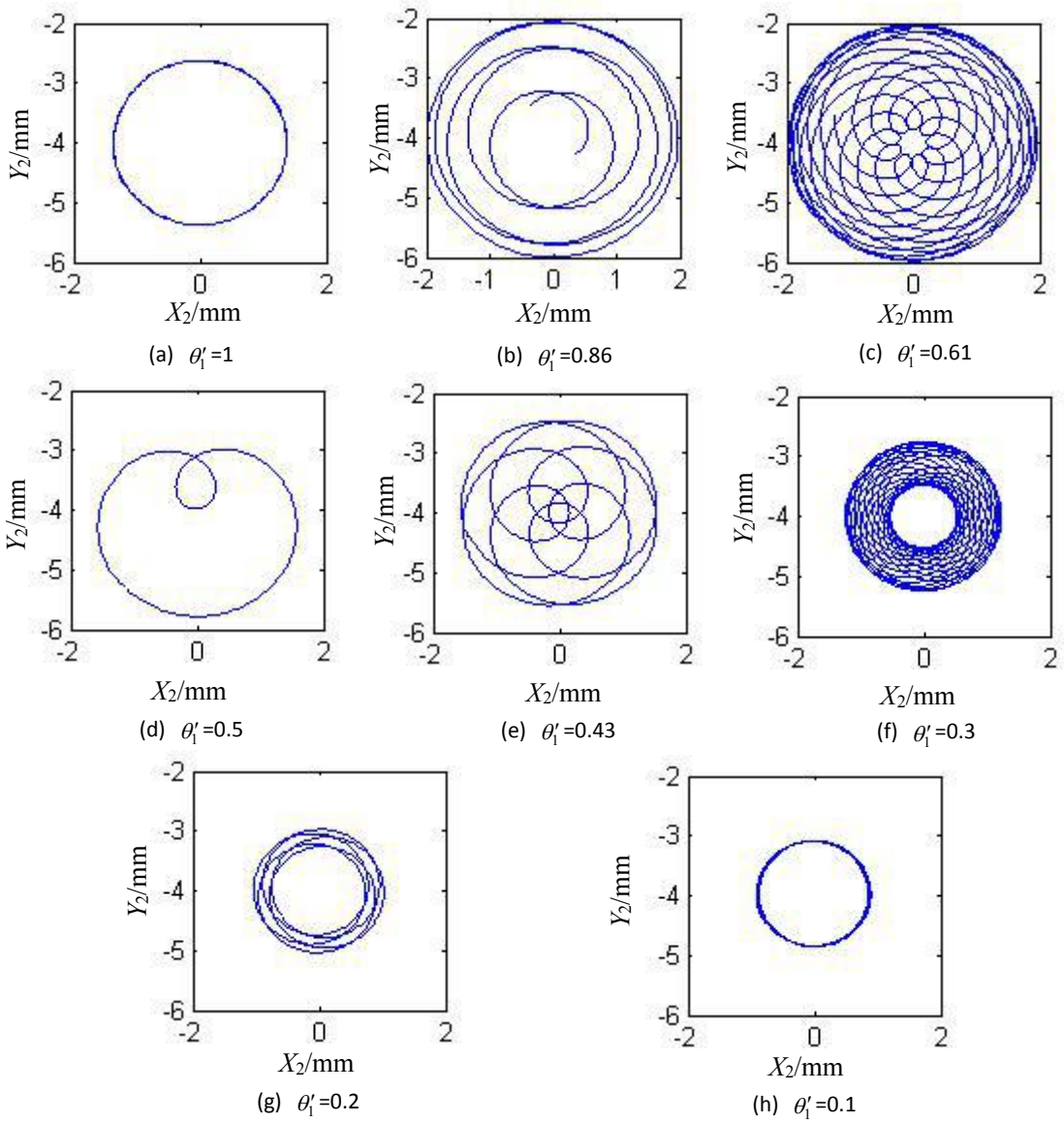

Figure 13 The trajectory of the disc at different θ_1'

Figure 13 is the disc trajectory at different θ_1'. With the decreases of θ_1', the trajectory changes from 'circular' to 'double ring' and then to 'circular'. The inner circle of 'double ring' gradually becomes small and then gradually becomes large. The outer circle of 'double ring' keeps getting small. The phenomenon of the 'double ring' should be caused by the difference of θ_1'. The reason why the outer circle is smaller is that the centrifugal force is smaller due to the reduction of θ_1'.

4. Experimental research

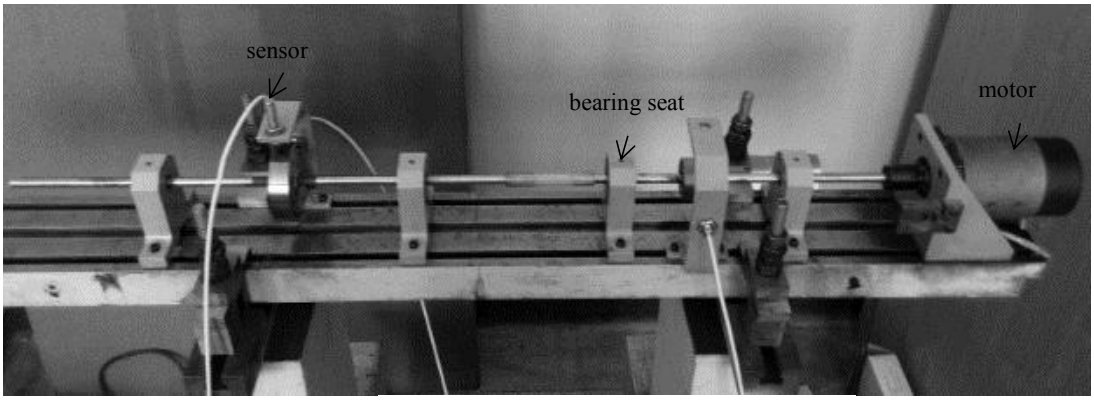

Figure 14 ZT-3 rotor experimental platform

The experimental system is composed of ZT-3 rotor experiment platform, Bentley displacement sensor and MULLER-BBM acquisition system. Figure 14 is the diagram of ZT-3 rotor experimental platform. The experimental platform consists of the power output system and the rotor system with loose disc. The flexible coupling is used as the demarcation point, the right half part is the power output system which consists of a motor, a joint coupling, a rotating shaft, a bearing seat, a flexible coupling, and a phase bonder. The right side of the flexible coupling is connected to a 320mm shaft and the left side is connected to a 500mm shaft. Both ends of the shaft are supported by sliding bearings. The main function of the flexible coupling is to make the power output system only output torque but not transverse or longitudinal vibration, thus the flexible coupling ensures the accuracy of the experimental results of the rotor system with loose disc. The main function of the phase bonder is to measure the rotational frequency of the shaft through an eddy current sensor. The motor in the experimental platform is a DC motor with the output power of 250W. By adjusting the governor, the motor can be adjusted in the range of 0 ~ 10000r / min. The left half part is a rotor system with loose disc, which consists of a rotating shaft, two bearing seats, and a disc. The shaft diameter is 9.5 mm, the disc mass is 0.612 kg, the outer diameter of the disc is 76.2 mm, and the distance between the centers of the two bearing seats is 422 mm.

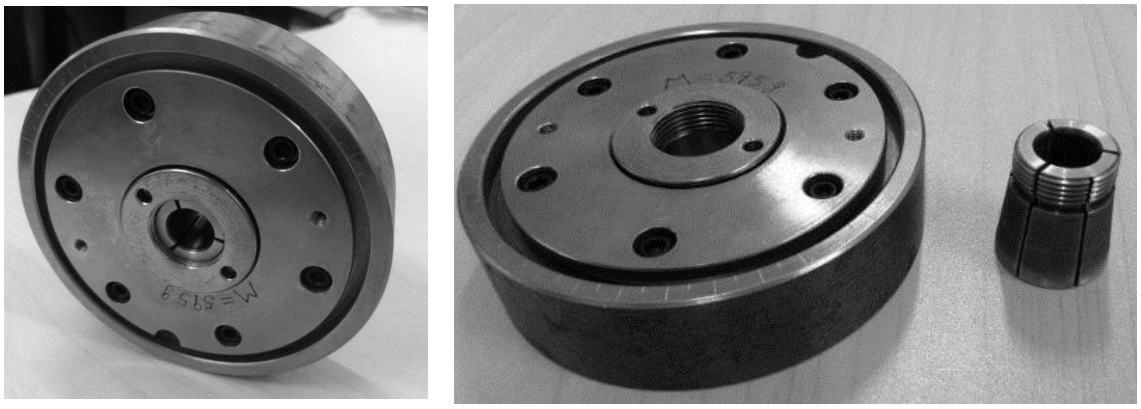

Figure 15 Structure diagram of the loose disc

This experiment analyzed the vibration characteristics of the rotor system with loose disc. Figure 15 is structure diagram of the loose disc. The structure of the disc consists of the inner ring and the outer ring. The two parts are assembled together by a tapered face and the pressing force is provided by the threads. When the thread rotates clockwise, the inner ring and the outer ring are pressed by the taper surface contact, so that the inner diameter of the inner ring reduces. Therefore, it is only necessary to rotate the thread clockwise to fix the disc on the rotating shaft.

4.1 The analysis of time-frequency characteristics

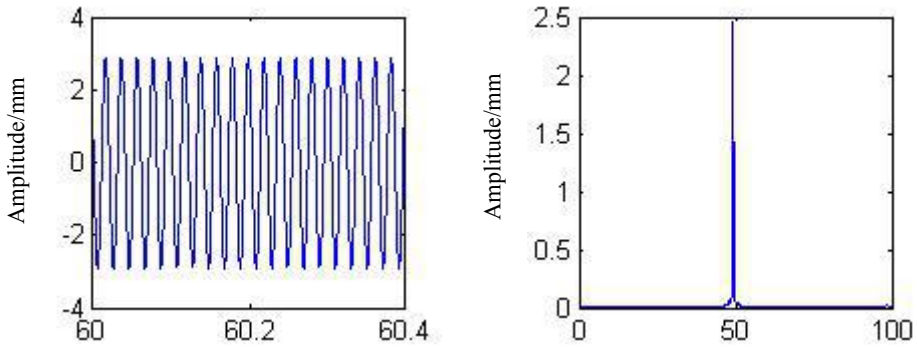

(a) Waveform (b) Spectrogram

Figure 16: The waveform and spectrogram of *x*-direction when the disc and the shaft at the same speed

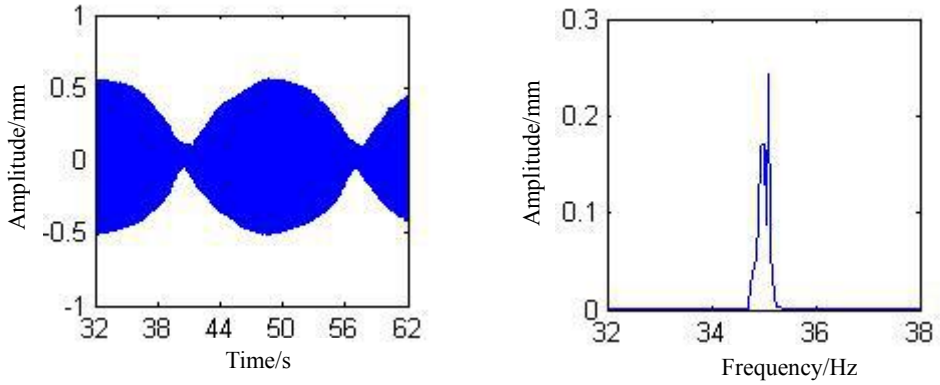

(a) Waveform (b) Spectrogram

Figure 17: The waveform and spectrogram of *x*-direction when the speed of the disc and the speed of the shaft is close

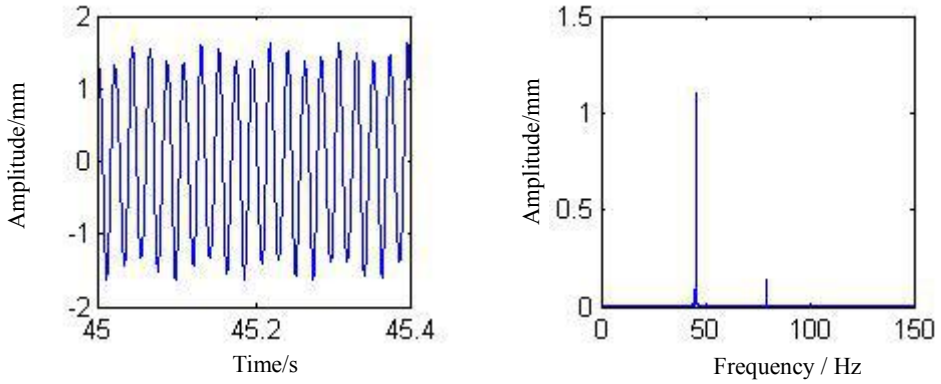

(a) Waveform (b) Spectrogram

Figure 18 The waveform and spectrogram of *x*-direction when the disc and the rotating shaft have a large difference in rotation speed.

The experimental results are shown in Figs 16-18 under several situations. When the rotating disc run at the same speed as the rotating shaft, and when the disc and the rotating shaft have a large difference in rotation speed, the collision frequency is mainly composed of one frequency component, the latter also contains high frequency multiplication components. When the rotational speed of the disc and the rotational speed of the shaft is close, the phenomenon of beating vibration occurs in the *x* direction of the disc, the collision frequency is mainly composed of low frequency components. Both the waveform and the spectrogram are similar to the simulation results. The spectrogram only includes the rotating frequency of the rotating disc and rotating shaft, and there is no collision frequency of the disc-shaft. The waveform diagram shows vibration phenomenon appears when the speed of the disc and the speed of the shaft is close.

4.2 The analysis of motion trajectory

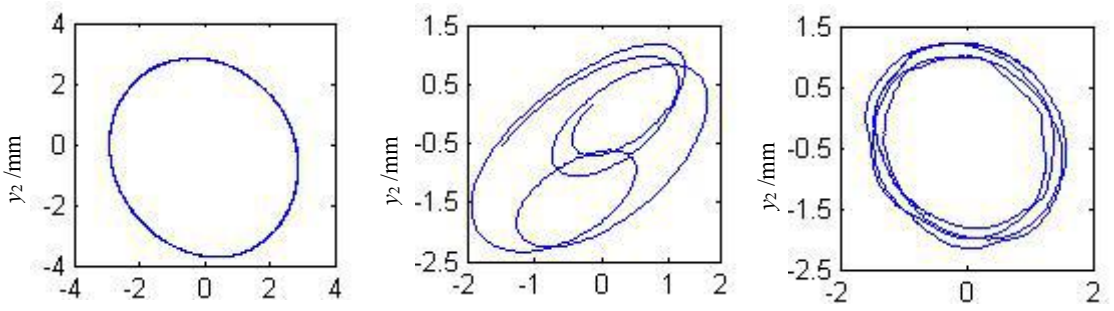

(a) θ_1'=1 (b) θ_1'=0.7 (c) θ_1'=0.5

Figure 19 The trajectory diagram of the disc at different θ_1'

Figure 19 is the trajectory diagram of the disc at different θ_1'. When the disc and the shaft run at the same speed, the motion trajectory is basically 'circular'. As the decreases of relative speed between the disc and shaft, the trajectory changes from 'circular' to 'double ring' then to 'circular'. When θ_1' decreases, the inner circle of the 'double ring' becomes small and then becomes large, and the outer circle becomes small. The experimental results are consistent with the simulation results. Experiments results show that the simulation model is reasonable.

5. Conclusion

In this paper, considering the microscopic surface topography, a dynamic contact model of the rotor system with loose disc is established. The effects of Ω, C, H, ξ_2 and ξ_3 on the motion state of the rotating disc are discussed and the time-frequency characteristics of the disc and the disc trajectory are discussed. And experimental results were used to verify the simulation results.

(1) The rotation state of the disc is affected by the rotation speed of the shaft, the contact stiffness, the gap, the damping of the disc, and the rotational damping. The rotor system with slight failure is more stable, which is in line with objective and practical.

(2) The disc spectrogram in the x direction contains the rotation frequency of the disc and the rotation frequency of the shaft, and no the collision frequency of disc was found. When the rotating disc run at the same speed as the rotating shaft, and when the disc and the rotating shaft have a large difference in rotation speed, the collision frequency is mainly composed of one frequency component, the latter also contains high frequency components. When the rotational speed of the disc and the rotational speed of the shaft is close, the beating vibration phenomenon of the disc occurs in the x direction, and the similar beating vibration phenomenon occurs periodically in the displacement waveform of the disc-shaft. The collision frequency is mainly

composed of low frequency components.

(3) When the disc and shaft run at the same speed, the trajectory of the rotating disc is ‘circular’. When the rotational speed of the disc approaches the shaft, the trajectory of the rotating disc is ‘double ring’. When the speed difference between the disc and shaft is large, the trajectory of the rotating disc changes to ‘circular’. As the decreases of relative speed between the disc and shaft, the inner circle of ‘double ring’ gradually becomes small and then becomes large. However, the outer circle of ‘double ring’ is always small. The difference in the rotational speed of the disc and the rotating shaft results in the appearance of the ‘double ring’ trajectory. The rotating speed of the disc is getting lower, and the centrifugal force provided is getting smaller. The outer circle of the ‘double ring’ has been getting smaller.

6. Declarations

Availability of data and material

The raw data required to reproduce these findings cannot be shared at this time as the data also forms part of an ongoing study.

Competing interests

The authors declare no competing financial interests.

Founding:

This work was supported by a grant from National Natural Science Foundation of China (No. 51675258, 51875301, 51075372) and National Key Laboratory of Mechanical Systems and Vibration (MSV201914).

Authors' contributions

The author’ contributions are as follows: ZL conceived and designed the study; FQ and JL wrote the manuscript; WL,DW and FC were in charge of the whole trial.

References

[1] Ma H, Zhang Z, Tai XY, Wen BC. Dynamic Characteristic Analysis of a Rotor System With Pedestal Looseness Under Two Load Case. Proceedings of the CSEE,2012,32(26):132-137+158.

[2] Sun CY, Yang R, Chen YS, Hou L. Modeling and experiment verification of a casing-dual-rotor high-dimensional system. Journal of Vibration and Shock,2018,37(18):152-157.

[3] Zhang J, Wen BC. A Study of Frequency Characteristics of Rotor System with Pedestal Looseness at Two Supports. China Mechanical Engineering,2008(01):68-71.

[4] Lu YJ, Ren ZH, Chen H, WenBC. Study on Looseness and Impact-Rub Coupling Faults of Vertical Dual-disc Over-Hung Rotor-Bearing System. Journal of Vibration, Measurement & Diagnosis,2007(02):102-107+169.

[5] Jiang M, Wu JG,Peng XS, Li XJ. Nonlinearity measure based assessment method for pedestal looseness of bearing-rotor systems. Journal of Sound and Vibration,2017,411:232-246.

[6] Cao SQ. Huang YM. An Improved Genetic Algorithm for Pedestal Looseness Parameter Identification in Rotor-Bearing Systems. Journal of Vibration, Measurement & Diagnosis,2018,38(03):446-453.

[7] Xu HZ, Wang NF, Jiang DX. Bearing pedestal looseness dynamic model of dual rotor system and fault feature. Journal of Aerospace Power,2016,31(11):2781-2794.

[8] Yang Y, Yang YR, Cao DQ, Chen G, Jin YL. Response evaluation of imbalance-rub-pedestal looseness coupling fault on a geometrically nonlinear rotor system. Mechanical Systems and Signal Processing, Volume 118, 1 March 2019, Pages 423-442

[9] Cao QS, Xiang Q, Xiong GL. Incremental Harmonic Balance Method For The Study of Support Looseness Fault's Characteristics. Journal of Mechanical Strength, 2015(6):999-1004.

[10] Cao HR, Shi F, Li YM, Li BJ, Chen XF. Vibration and stability analysis of rotor-bearing-pedestal system due to clearance fit. Mechanical Systems and Signal Processing Volume 133,1 November 2019, 106275.

[11] An XL, Jiang DX, Li SH, Zhao MH. Application of the ensemble empirical mode decomposition and Hilbert transform to pedestal looseness study of direct-drive wind turbine. Energy,2011,36(9):5508-5520.

[12] Behzad M, Asayesh M. Vibration analysis of rotating shaft with loose disk, IJE Transactions B [J]: Applications, 2002, 15(4): 385-393.

[13] Behzad M, Asayesh M. Numerical and experimental investigation of the vibration of rotors with loose discs, Proc. IMechE Part C. Mechanical Engineering Science,2010, 224:85-94.

[14] Yang GX, Xie JL, Zhou SX, Xiao N, Xie YY. Research on the Influence of Axle Design Parameters on Contact Pressure between Axle and Hub. Journal of the China Railway Society,2009,31(03):31-35.

[15] Zhong weiyan, Ren yongsheng, Gao F, Liu L, Liu J. Finite Element Simulation of Dynamic Characteristics of Composite Thin-walled Shaft Rotor System. Journal of Shandong University of Science and Technology (Natural Science),2016,35(05):87-95.

[16] Ll ZP, Luo YG, Yao HL, Wen BC. Dynamics and Fault Characteristics of Rotor-Bearing System with Pedestal Looseness. Journal of Northeastern University (Natural Science), 2002, 23(11):1048-1051.

[17] Guo RD, Xue S, Zheng LX, Deng AL, Liu L. Fracture failure analysis of DY08Aluminum alloy elastic coupling. Engineering Failure Analysis,2019,104:1030-1039.

[18] Wang H, Han QK, Zhou DN. Nonlinear dynamic modeling of rotor system supported by angular contact ball bearings. Mechanical Systems and Signal Processing,2017,85:16-40.

[19] Ulrich Ehehalt, Oliver Alber, Richard Markert, Georg Wegener. Experimental observations on rotor-to-stator contact. Journal of Sound and Vibration,2019,446:453-467.

[20] Zhang H, Zhang X, He NN. Rotor dynamic analysis of small vehicle gasoline turbocharger in semi-floating bearings. Journal of Beijing Institute of Technology,2011,20(04):502-508.

[21] Liao MF,Li Y, Song MB, Wang SJ. Dynamics Modeling and Numerical Analysis of Rotor with Elastic

Support/Dry Friction Dampers. Transactions of Nanjing University of Aeronautics and Astronautics,2018,35(01):69-83.

[22] Zhang J, Li H, Wen BC. On the Pedestal Looseness of Dynamic Oil Film-Rotor System. Journal of Northeastern University (Natural Science), 2003, 24(10):880-880.

[23] Yang L, Yang SP, Wang JJ, Liu YQ. Nonlinear Vibration Analysis of Locomotive Rotor System. Journal of Mechanical Engineering,2018,54(18):97-104.